

Electronic Supplementary Information

Pressure-enhanced polarisation in polar perovskite-like $[C_2H_5NH_3]Na_{0.5}Cr_{0.5}(HCOO)_3$ metal-organic framework

by M. Ptak *et al.*

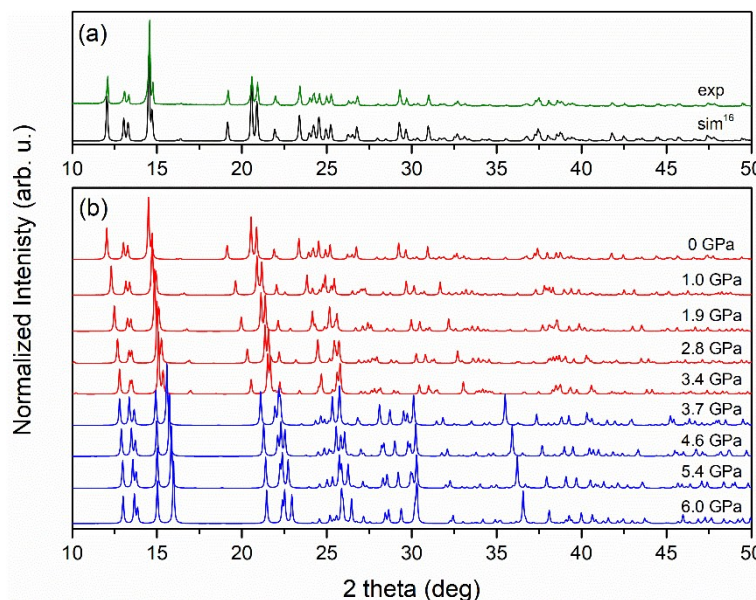


Fig. S1. The experimental (exp.) XRD powder pattern of EtANaCr compared to simulated one based on the cif file published previously (sim)¹ (a) and the pressure evolution of simulated XRD patterns based on single-crystal pressure experiment exhibiting a structural phase transition occurring in the 3.4–3.7 GPa range (b).

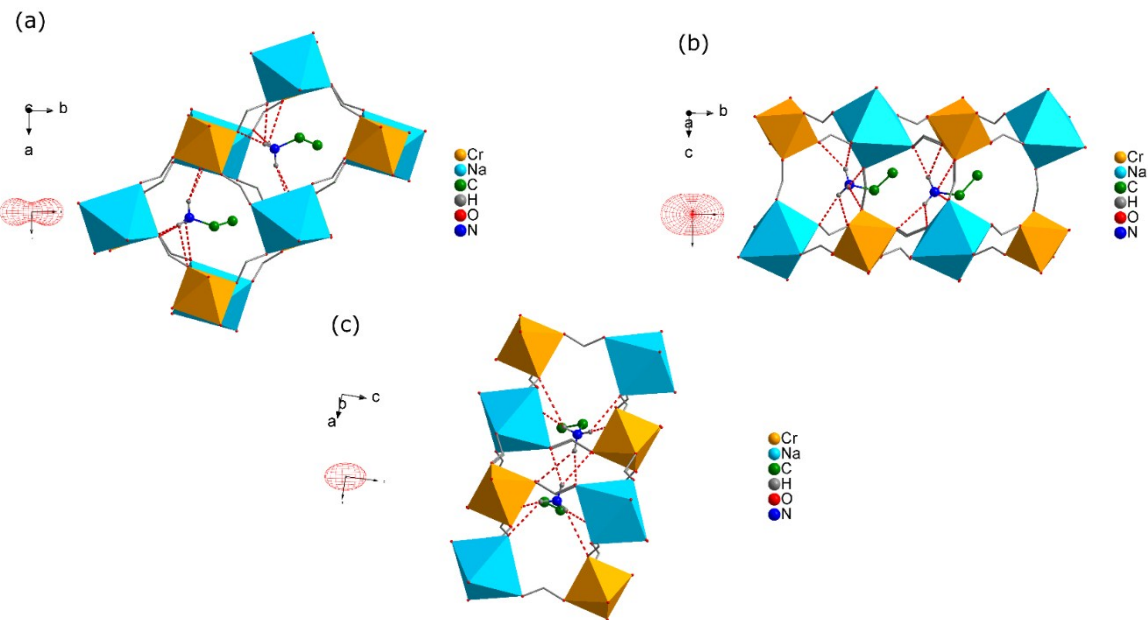


Fig. S2. The crystal structure of phase I along c (a), a (b) and b (c) directions together with the HBs (red dotted lines) and graphical representations of the compressibility (κ) indicatrix calculated using PASCAL program.² The aliphatic H-atoms are omitted for clarity.

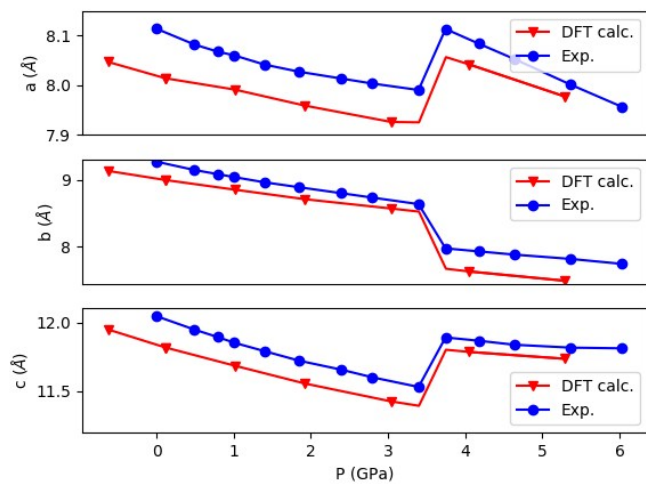


Fig. S3. Calculated (red triangles) and experimentally determined (blue circles) unit cell parameters as a function of pressure.

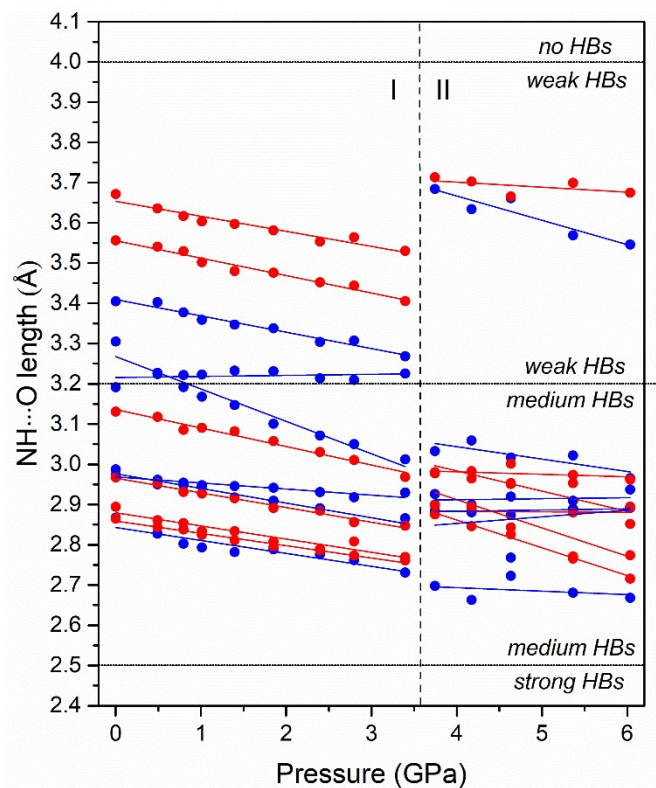


Fig. S4. The change of N–H···O distance with the increasing pressure. The dashed vertical line represent the pressure, where the structural phase transition takes place. The horizontal lines indicate the conventional classification of HBs.

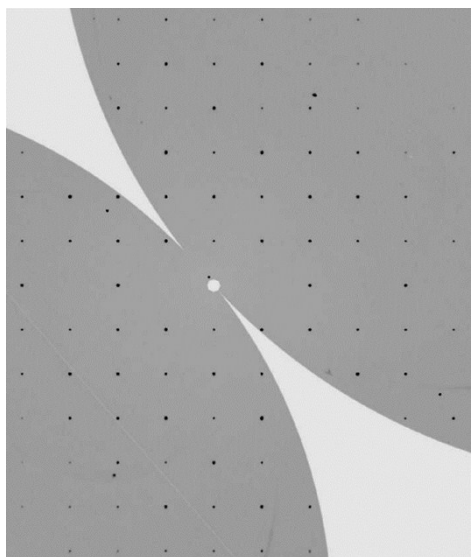


Fig. S5. The $hk0$ plane in reciprocal space for EtANaCr-I phase at 3.40 GPa.

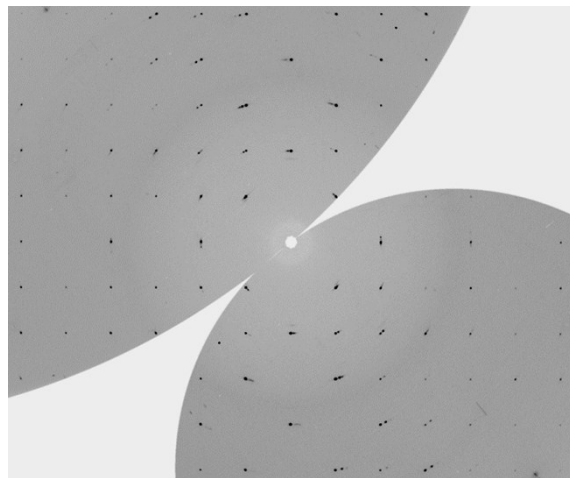


Fig. S6. The $hk0$ plane in reciprocal space for EtANaCr-II phase at 3.75 GPa.

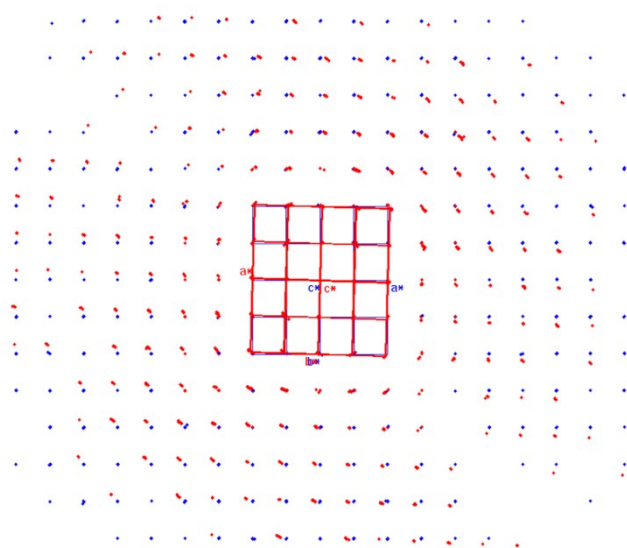


Fig. S7. The two twin domains (indicated in red and blue) formed in the high-pressure phase of EtANaCr (at 3.75 GPa), viewed in reciprocal space using *CrysAlisPro*.³ The domains are related by a 180° rotation about the $(0\ 1\ 0)$ axis.

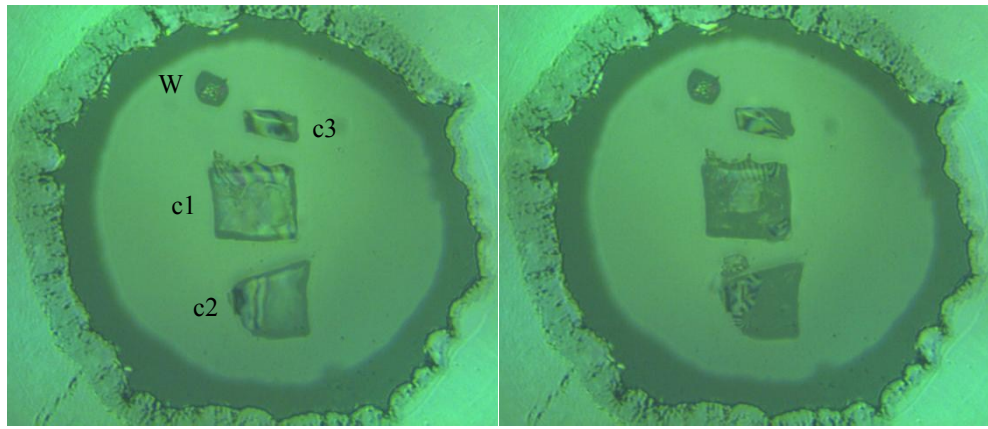


Fig. S8. Three crystals (c1–c3) of EtANaCr loaded in the gasket, along with a piece of tungsten (W) for centering purposes. The left figure is taken at 3.40 GPa before the phase transition, and the right figure is at 3.75 GPa within the high-pressure phase.

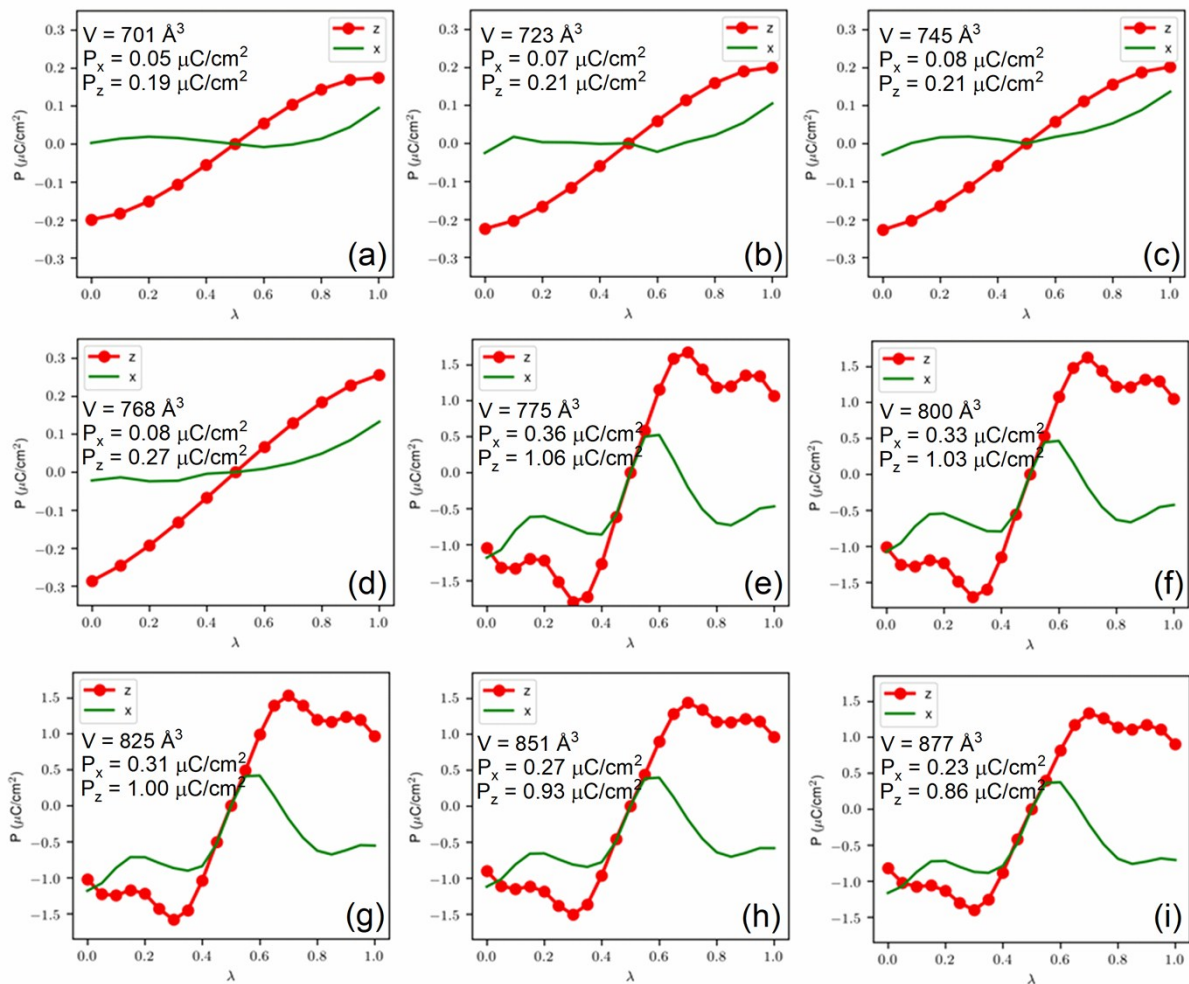


Fig. S9. The change in polarization for different volumes of the high-pressure $P2_1/n$ phase (a-d) and the low-pressure Pn phase (e-i) as a function of λ , where λ is the normalised amplitude of the atomic distortion connecting the two structures with polarisations $+P_s$ and $-P_s$.

Tab. S1. Crystallographic details of EtANaCr at 0 and 3.7 GPa loaded in neon.

	Phase I	Phase II
Crystal data		
Chemical formula	C ₁₀ H ₂₂ CrNaN ₂ O ₁₂	C ₁₀ H ₂₂ CrNaN ₂ O ₁₂
M _r	437.28	437.28
Crystal system, space group	Monoclinic, <i>Pn</i>	Monoclinic, <i>P2₁/n</i>
pressure (GPa)	0	3.7
<i>a</i> , <i>b</i> , <i>c</i> (Å)	8.1137(3), 9.2703(4), 12.045(5)	8.1131(6), 7.9779(6), 11.891(5)
α, β, γ (°)	90, 91.173(9), 90	90, 86.024(18), 90
<i>V</i> (Å ³)	905.8(4)	767.8(3)
<i>Z</i>	2	2
Crystal size (μm)	60×50×30	50×50×20
Data collection		
No. of reflections		
measured	3385	5486
unique	2565	2791
unique with <i>I</i> > 2σ	1938	991
<i>R</i> _{int}	0.0245	0.0386
Refinement		
No. of parameters	234	124
<i>R</i> ₁ [<i>I</i> > 2σ(<i>I</i>)]	0.0472	0.0399
w <i>R</i> ₂ (all data)	0.1365	0.0930
Δρ _{max} , Δρ _{min} (e Å ⁻³)	0.36, -0.51	0.23, -0.28

Tab. S2. Raman pressure intercepts (ω_0) and coefficients (α) for the two phases of EtANaCr obtained from the linear fits on the data together with proposed assignment.^a

Mode	Phase I (LP)		Phase II (HP)		Assignment
	ω_0 (cm ⁻¹)	dω/dP (cm ⁻¹ /GPa)	ω_0 (cm ⁻¹)	dω/dP (cm ⁻¹ /GPa)	
1	3018.5	6.36	3003.0	9.80	v _{as} (CH ₃)+v _{as} (CH ₂)
2	2950.1	4.01	2962.8	6.17	v _{as} (CH ₃)+v _{as} (CH ₂)
3	1670.0	5.46	1682.9	0.42	v ₄ (HCOO ⁻)+δ _{as} (NH ₃)
4	1456.6	4.38	1463.1	2.68	δ(CH ₃)+δ(CH ₂)
5	1375.2	2.55	1368.6	7.66	v ₅ (HCOO ⁻)
6	1054.8	5.47	1042.7	7.10	v ₆ (HCOO ⁻)+v _{as} (CCN)
7	876.5	4.61	882.0	3.52	v _s (CCN)
8	339.8	9.69	346.3	6.87	T'(Cr ³⁺)
9	232.2	4.96	194.4	13.56	T'(Na ⁺)+T(HCOO ⁻)
10	186.9	7.32			L(HCOO ⁻)
11	139.1	9.19	135.8	12.07	L(HCOO ⁻)
12	122.6	7.58	115.0	9.33	L(HCOO ⁻)
13	106.2	8.29	138.0	0.73	L(HCOO ⁻)
14	69.0	9.10	94.0	5.33	T'(EtA ⁺)+L(EtA ⁺)
15	56.8	5.12	59.2	6.92	T'(EtA ⁺)+L(EtA ⁺)
16	43.0	3.96	43.8	5.24	T'(EtA ⁺)+L(EtA ⁺)
17	39.3	0.43	40.2	0.30	T'(EtA ⁺)+L(EtA ⁺)
18	26.9	1.15			T'(EtA ⁺)+L(EtA ⁺)
19	23.6	1.20	27.5	0.35	T'(EtA ⁺)+L(EtA ⁺)
20	21.8	1.14	25.1	0.11	T'(EtA ⁺)+L(EtA ⁺)

^aKey: v_s, v_{as}, δ, δ_s, δ_{as}, v₄, v₅, v₆, T' and L denote symmetrical stretching, antisymmetric stretching, bending, symmetric bending, antisymmetric bending, the antisymmetric CO stretching, the CH in-plane bending, the CH out-of-plane bending, translational and librational mode.

Tab. S3. Calculated and experimentally determined unit cell parameters at 0 GPa.

Exp. (297 K) ¹⁶	DFT
----------------------------	-----

Space group	<i>Pn</i>	<i>Pc</i>
<i>a</i> (Å)	8.113	8.018
<i>b</i> (Å)	9.2703	9.023
<i>c</i> (Å)	12.045	11.842
β (°)	91.17	92.9
V (Å ³)	905.8	855.68

Tab. S4. Hydrogen bonding parameters extracted from DFT calculations of the low-pressure phase (*Pn* space group).^a

LP phase	d(N···O) (Å)	d(H···O) (Å)	\angle (NH···O) (°)	d(N···O) (Å)	d(H···O) (Å)	\angle (NH···O) (°)
	P = 0 GPa		P=3 GPa			
N1–H···O1	2.86	1.84	164	2.75	1.71	171
N1–H···O2	2.76	1.71	171	2.71	1.66	170
N1–H···O3	2.80	1.78	161	2.75	1.75	158
N1–H···O4	3.21	2.40	133	3.19	2.44	128
N1–H···O5	3.31	2.72	115	3.21	2.64	113
N1–H···O6	3.25	2.48	129	3.08	2.31	129
N2–H···OA	2.74	1.70	166	2.67	1.62	168
N2–H···OB	2.76	1.70	176	2.70	1.64	177
N2–H···OC	2.89	1.85	175	2.81	1.77	175
N2–H···OD	3.56	2.76	132	3.49	2.71	130
N2–H···OE	3.52	2.79	125	3.41	2.72	123
N2–H···OF	3.11	2.45	120	3.00	2.35	119

^aKey: d, distance; \angle , angle; °, deg.

Tab. S5. Hydrogen bonding parameters extracted from DFT calculations of the high pressure phase (*P2₁/n* space group).^a

HP phase	d(NH···O) (Å)	d(H···O) (Å)	\angle (NH···O) (°)
	P = 4 GPa		
N1–H···O1	2.80	1.90	143
N1–H···O2	2.80	1.80	158
N1–H···O3	2.71	1.65	175
N1–H···O4	2.93	2.19	127
N1–H···O5	3.03	2.27	129
N1–H···O6	3.60	2.81	131

^aKey: d, distance; \angle , angle; °, deg.

References

- (1) Ptak, M.; Mączka, M.; Gągor, A.; Sieradzki, A.; Bondzior, B.; Dereń, P.; Pawlus, S., *Phys. Chem. Chem. Phys.* 2016, **18**, 29629–29640.
- (2) Cliffe, M. J.; Goodwin, A. L., *PASCal*: A Principal Axis Strain Calculator for Thermal Expansion and Compressibility Determination. *J. Appl. Crystallogr.* 2012, **45**, 1321–1329.
- (3) Rigaku Oxford Diffraction CrysAlisPro Software System, Version 1.171.39.46, Rigaku. 2018.